Improved droplet breakup models for spray applications

Affiliations

Dionisis Stefanitsis[*1,2], George Strotos[3], Nikolaos Nikolopoulos[1], Emmanouil Kakaras[1], Manolis Gavaises[2]

[1]Centre for Research and Technology Hellas/Chemical Process and Energy Resources Institute (CERTH/CPERI), Egialeias 52, Marousi, Greece

[2]City University London, School of Engineering and Mathematical Sciences, Northampton Square, EC1V 0HB London, UK

[3]Technological Educational Institute of Thessaly, Mechanical Engineering Department, 41110 Larissa, Greece

[*]Corresponding author: stefanitsis@certh.gr

gstrot@teilar.gr, n.nikolopoulos@certh.gr, ekak@central.ntua.gr, M.Gavaises@city.ac.uk

Abstract

The current study examines the performance of two zero-dimensional (0D) aerodynamically-induced breakup models, utilized for the prediction of droplet deformation during the breakup process in the bag, multi-mode and sheet-thinning regimes. The first model investigated is an improved version of the widely used Taylor analogy breakup (TAB) model, which compared to other models has the advantage of having an analytic solution. Following, a model based on the modified Navier-Stokes (M-NS) is examined. The parameters of both models are estimated based upon published experimental data for the bag breakup regime and CFD simulations with Diesel droplets performed as part of this work for the multi-mode and sheet-thinning regimes, for which there is a scarcity of experimental data. Both models show good accuracy in the prediction of the temporal evolution of droplet deformation in the three breakup regimes, compared to the experimental data and the CFD simulations. It is found that the best performance of the two is achieved with the M-NS model. Finally, a unified secondary breakup model is presented, which incorporates various models found in the literature, i.e. TAB, non-linear TAB (NLTAB), droplet deformation and breakup (DDB) and M-NS, into one equation using adjustable coefficients, allowing to switch among the different models.

Keywords

droplet breakup models; droplet deformation; TAB; CFD;

Nomenclature

Roman symbols		ε	Density ratio [-]
C_d	Viscosity coefficient [-]	μ	Dynamic viscosity [kg/(m·s)]
C_f	Pressure coefficient [-]	ρ	Density [kg/m^3]
C_k	Surface tension coefficient [-]	σ	Surface tension [N/m]
D	Droplet diameter [m]	**Subscripts/Superscripts**	
E	Energy [J]	*	Non-dimensional quantity

F	Force [N]	*0*	Initial
f	Adjustable parameter [-]	cm	Center of mass
h	Rim thickness [m]	*cr*	Cross-stream
k	Curvature [1/m]	*d*	Droplet
m	Mass [kg]	*def*	Deformation
n	Pressure exponent [-]	g	Gas
Oh	Ohnesorge number [-]	*kin*	Kinetic
P,p	Pressure [Pa]	*L*	Liquid phase
R	Droplet radius [m]	*r*	Radial
r	Radial coordinate [m]	*ref*	Reference
Re	Reynolds number [-]	*rel*	Relative
S	Surface area [m^2]	*st*	Surface tension
T	Stress component [N/m^2]	*surf*	Surface
t	Time [s]	*press*	Pressure
t_{sh}	Shear breakup timescale [s]	*vis*	Viscous
U,u	Velocity [m/s]	**Abbreviations**	
W	Work [W}	*Bag-NS*	Bag Navier-Stokes
y	Dimensionless droplet deformation [-]	*BTB*	Bag-type-breakup
$\dot{y}$	Dimensionless deformation rate [-]	*DDB*	Droplet deformation and breakup
$\ddot{y}$	Dimensionless deformation acceleration [-]	DMTAB	Double mass Taylor analogy breakup
x	Axial coordinate [m]	*M-NS*	Modified Navier-Stokes
Greek symbols		*NLTAB*	Non-linear Taylor analogy breakup
α	Rate of stretching [-]		

1 Introduction

Research on liquid sprays has received a lot of attention due to their numerous applications, ranging from pharmaceutical to internal combustion engines [1]. Modeling of such systems is difficult due to the complex physical phenomena involved in them, also occurring in various time and length scales. One way to model as fast as possible such systems with acceptable accuracy, is by utilizing macroscopic CFD spray codes following the Lagrangian approach, which estimate the trajectory of each droplet as well as its deformation [2]. The former can be calculated using the drag coefficient of each droplet and the droplet motion equation. The drag coefficient of deforming droplets has been thoroughly studied in [3-17]. The droplet deformation, which is the focus of this study, is usually quantitatively described by the cross-stream droplet diameter (Figure 2) and several models have been developed for its estimation as a function of time. These can be classified into empirical correlations based on experimental observations and semi-analytic/theoretical models, which are based on physical principles.

Various studies in the literature conducted experiments of aerodynamic droplet breakup and based on their results they proposed empirical correlations for the prediction of the droplet deformation as a function of the non-dimensional time. These correlations can be written in the general form of $y=$

$c_0+c_1(t^*)^{c2}+c_3(t^*)^2$, where y is the non-dimensional deformation (Figure 2), whilst the coefficients c_0, c_1, c_2 and c_3 are summarized for each study in Table 1, along with their range and conditions of applicability. Apparently, these correlations perform quite well when compared against the experimental data that they were based upon, and the question arises is if they also perform well against other data at a) similar conditions and b) at different breakup modes. This is addressed in Appendix A in which the model results are compared against the experimental data of [12, 18-22] in the three main breakup regimes (bag, multi-mode and sheet-thinning) for Weber numbers in the range of 15 to 101. In the bag breakup regime (*We*=15-20) the model of Chou and Faeth [18] shows the best agreement with the experimental data, in the multi-mode regime (*We*=52.6) that of Cao et al. [23] and in the sheet-thinning regime the model of Gel'fand et al. [24] (*We*=101). None of the models is able to accurately predict the droplet deformation in all the examined regimes.

Table 1. Summary of empirical correlations for droplet deformation.

General equation: $y=c_0+c_1(t^*)^{c2}+c_3(t^*)^2$							
					Conditions of applicability[*1]		
Study	c_0	c_1	c_2	c_3	**Non-dimensional numbers**	**Breakup mode**	**Time range**
Gel'fand et al. [24]	*1*	*1- We/We_{cr}*	*1*	*0*	*We=24-180*	Bag, multi-mode, sheet-thinning	*$t^*\leq1.5$*
Hsiang and Faeth [20]	*1*	*$0.23We^{1/2}$*	*1*	*0*	*$We=4\text{-}10^5$*	Deformation up to sheet-thinning	-
Chou and Faeth [18]	*1* *1.43* *-2.51*	*0.5* *-0.18* *1.79*	*1* *1* *1*	*0* *0.25* *0*	*We=13-20, Oh<0.05*	Bag	*$t^*\leq2$* *$2\leq t^*\leq4$* *$4\leq t^*\leq6$*
Cao et al. [23]	*1* *0.59*	*0* *1.34*	*0* *1*	*0* *0*	*We=28-41, Oh<0.003*	Multi-mode	*$t^*\leq0.3$* *$0.3<t^*<0.99$*
Zhao et al. [25]	*1*	*0.54*	*1.67*	*0*	*We=16-26, Oh<0.4*	Multi-mode	*$t^*\leq1.5$*

[1]Refers to the conditions of the experiments that the corresponding model was based upon. The models are generally valid for low *Oh* numbers

Turning now to the theoretical and semi-analytical models for the droplet deformation and breakup, the majority of them is based on one of the two basic principles: i) conservation of momentum or ii) conservation of energy. O'Rourke and Amsden [26] proposed the so called Taylor analogy breakup (TAB) model, in which the droplet is assumed to oscillate between its initial spherical shape and that of the deformed oblate shape. The droplet oscillates similarly to a mass-spring-damper system with the surface tension force being the restoring force, the viscosity representing the damping force and the aerodynamic force being the external force acting on the droplet. Lee et al. [27] indicated later

that the TAB model shows good agreement with the experiment of Krzeczkowski [22] for the breakup of a water droplet with *We*=101. Later, Kim et al. [28] tuned these coefficients to match the results of their experiments for Diesel droplets at *We* numbers in the range of 9.6 up to 26.6. Finally, Marek [29] introduced another degree of freedom to the mathematical formulation of TAB, so as to include also the translational motion of the droplet. A second mass was added to the system, which could move and oscillate independently, and thus the system resembled the system configuration of a double mass-spring-damper giving the name to the model as double mass TAB (DMTAB). The DMTAB is applicable to the deformation and bag breakup regimes and its advantage over the TAB model is that it can treat cases with low density ratios (ε) and high *Oh* numbers, in which the droplet translational velocity changes significantly.

Another approach on breakup models still based on the momentum balance, is that of Villermaux and Bossa [30], in which they utilized the inviscid Navier-Stokes equations in cylindrical coordinates for the liquid droplet and the quasi-steady conservation of momentum and mass for the gas phase, to estimate the temporal variation of the droplet deformation in the bag breakup regime. Opfer et al. [31] used the momentum balance on the droplet as well, which was approximated by a cylinder of the same radius, to predict the droplet deformation in the bag breakup regime. Later, Kulkarni and Sojka [19] added the effect of viscosity to the model of [30] and it showed good agreement with their own experimental data for *We* numbers ranging from 13 up to 15.

Instead of utilizing the momentum balance on the droplet, Detkovskii and Frolov [32] and later Wang et al. [33, 34] utilized the equation of the linear strain of the droplet along its cross-stream axis to estimate the droplet deformation. They called the model BTB (bag-type breakup) and its results showed good agreement against the experimental data of [18, 22] in the bag breakup regime.

Regarding the theoretical models based on the conservation of energy, Ibrahim et al. [35] developed the so called deformation and breakup model (DDB), which is applicable to deforming droplets for *We* numbers greater than 20. Rimbert et al. [36] improved the DDB model by assuming potential flow around the droplet and extensional flow (i.e. with no shear) inside the droplet. The resulting model showed acceptable agreement with the experimental data of [22, 31] for *We* numbers equal to 11.5, 18.4 and 103.5, while the agreement was not good for the case of *We*=13.5. Schmehl and co-workers [37, 38] utilized the mechanical energy balance on the droplet to derive a non-linear differential equation similar to that of TAB, which they named non-linear TAB (NLTAB). This equation accounts for the modification of the aerodynamic forces imposed by the deformation of the droplet, and it showed good agreement with the experimental data of [21, 39] for the time variation of droplet deformation. Finally, Sichani and Emami [40] utilized the virtual work principle to describe the droplet deformation in the deformation and bag breakup regimes. The results of the model showed good agreement with the experimental data of [18, 21, 22, 41, 42] for *We* numbers ranging from 12.5 up to 20.

The aforementioned theoretical models are summarized in Table 2 along with their basic characteristics. In addition, the performance of selected models (TAB, DDB, NLTAB, Rimbert et al. [36] and Kulkarni and Sojka [19]) is evaluated by comparing their results with the experimental data of [12, 18-22] in the three breakup regimes (bag, multi-mode and sheet-thinning) for *We*=15-101, as presented in Appendix A. For *We*=15 the model of Kulkarni and Sojka [19] agrees well with the experimental data, while for *We*=52.6 and *We*=110 the DDB model gives the best results overall. For

117 *We*=20 all models deviate from the experimental data. Similar to the empirical models, none of the
118 examined theoretical models is able to accurately predict the droplet deformation in all the examined
119 regimes.
120
121 Table 2. Summary of theoretical and semi-analytical models for droplet breakup.

Model	**Basic principle**	**Droplet shape**	**Pressure distribution around the droplet**	**Internal circulation**	**Coupling with translational motion**	**Breakup condition**	**Adjustable parameters**	**Applicability *[1]**
TAB [43]	Momentum conservation	Ellipsoid	Uniform	No	No	$y_{cr}=2$	3	-
NLTAB [37, 38]	Energy balance	Ellipsoid	Spatial	Yes	No	$y_{cr}=1.8$ *and* $\dot{y}=0$ *or* $y_{cr}=2.1$	1	-
DMTAB [29]	Momentum conservation	Ellipsoid	Uniform	No	Yes	$y_{cr}=2$	*3*	*We*≤50, large and small ε and *Oh*
DDB [35]	Energy balance	Elliptic cylinder	Uniform	No	No	$y_{cr}=(We/2)/(6\pi)$	*0*	*We*>20
Rimbert et al. [36]	Energy balance	Ellipsoid	Spatial (potential flow)	Yes (homothetical deformation)	Yes	$y_{cr}=2$	0	-
BTB [32-34]	Linear strain equation	Ellipsoid	Uniform	No	No	$(B^{-1}+B^{5}-2B^{-4})/30>We$, $B=(3\pi/4)y$	1	10<*We*<35, *Oh*<0.1
Opfer at al. [31]	Momentum conservation	Cylinder	Spatial (parabolic)	No	No	-	2	11<*We*<25
Kulkarni and Sojka [19]	Momentum and mass conservation (Navier-Stokes)	Bag	Spatial (stagnation point)	No	No	-	1	12<*We*<16

Sichani and Emami [40]	Lagrange-type equations of motion	Bag	Spatial	Yes	No	$\frac{4}{3}\frac{1-K^{*2}}{y_1^2+y_2^2}$	*1*	*We*≤20, *Re*>100, *ε*>500,

[1]Applicability is based on the original paper proposing the model.
[2]*K* is a parameter; y_1 and y_2 are the deformations in both axes.

The aforementioned observations lead to the conclusion that there is a lack of a single accurate enough model for the prediction of droplet deformation for a wide range of *We* numbers in the three basic breakup regimes: i) bag, ii) multi-mode and iii) sheet-thinning. So far, the TAB model is widely used in spray codes due to its simplicity, since it has an analytic solution. However, it predicts purely oscillatory deformation for all breakup regimes, something that is not realistic (see Figures 4 to 6). On the other hand, the recently developed model of Kulkarni and Sojka [19] (termed as bag-Navier-Stokes or bag-NS for the remaining of the paper) predicts an exponential growth, which agrees well with experimental observations for the bag breakup mode, but it cannot be used to other breakup modes. The scope of the present work is to extend these two models. Nevertheless, it should be noted that an oscillatory deformation superimposed to an exponential function might result in a more accurate model, however, its implementation is complicated, possibly without significantly improving its performance compared to the models that follow one of the two approaches.

Regarding the TAB model, its coefficients are re-estimated to match the actual deformation, whilst the bag-NS is modified so it can be extended to other breakup modes and is termed as M-NS (modified Navier-Stokes). The parameters of both models are specified in each breakup regime, based both on experimental data available in the literature (*We*=15-20) and CFD simulations performed as part of this study (*We*=20-350). Finally, in Appendix B several breakup models (TAB, DDB, NLTAB and NS) are presented in a unified way using a common equation along with adjustable coefficients to switch to the different models (termed as unified secondary breakup model). It should be mentioned that this work focuses only on the effect of *We* number, while a sperate investigation is required for the effect of other non-dimensional numbers (*Oh*, *ε*, *Re*) as well as the effect of ambient temperature.

In the following sections, initially the computational setup and examined conditions of the CFD simulations are presented, followed by the description of the mathematical models of the TAB and M-NS models. It follows the presentation of the results of each model along with experimental data and the results of the CFD simulations. Finally, the conclusions and recommendations are summarized in the last section of the paper.

2 Computational setup and examined conditions

Apart from utilizing experimental data for the estimation of the model parameters, complimentary CFD simulations have also been performed. The CFD simulations are utilized for the derivation of the parameters of the improved TAB and M-NS models in the multi-mode and sheet-thinning regimes, in which there is a scarcity of experimental data to cover substantially the whole range of *We* numbers (*We*=21-350). In addition, the simulations provide useful information regarding the critical

deformation, which is necessary for the extraction of a breakup condition that is utilized in both breakup models.

The numerical CFD model solves the Navier-Stokes equations coupled with the Volume of Fluid (VOF) methodology [44] for tracking the interface between the liquid droplet and the surrounding gas. The surface tension forces are modelled with the Continuum Surface Stress (CSS) model of [45]. The simulations are performed in a two-dimensional axisymmetric domain with the commercial CFD tool ANSYS FLUENT v16 [46]. At low Reynolds numbers, such as those examined in this work (Table 4), the axisymmetric approximation has proven to be relatively accurate during the deformation stages of breakup [16, 47, 48]. Various User Defined Functions (UDFs) are employed for i) the adaptive local grid refinement technique around the liquid-gas interface [49], ii) the adaptive time-step scheme for the implicit VOF solver based on the velocity at the droplet interface [13], and iii) the moving mesh technique based on the average velocity of the droplet. The CFD model has been developed and validated in previous works for the case of aerodynamic droplet breakup [13, 16, 17, 50-53], as well as for other applications such as the free fall of droplet [49], the droplet impingement on a flat wall [54] or a spherical particle [55-57], and the droplet evaporation [13, 52, 58].

The 2-dimensional axisymmetric computational domain and boundary conditions are presented in Figure 1. The droplet is initially stagnant, while air flows from the left boundary with a constant velocity U_g, causing it to move and deform. The computational cells have a rectangular shape with a base grid resolution equal to 3cpR (cells per radius), while 6 levels of local grid refinement are applied to obtain the desired resolution of 192cpR around the liquid-gas interface. The resolution of 192cpR is adequate for the simulations of droplet breakup, since simulations with 48, 96, 192 and 384cpR have shown that the average drop velocity and deformation change less than 1% when a finer grid is used.

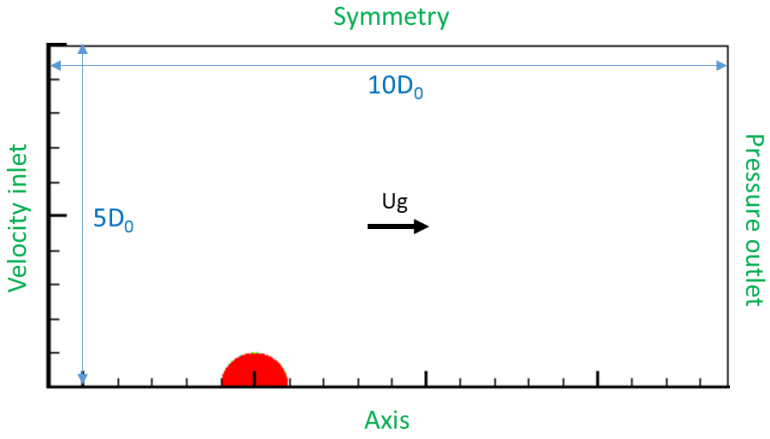

Figure 1. Computational domain and boundary conditions for the CFD simulations.

The liquid properties correspond to those of Diesel fuel, while the surrounding gas is air at temperature of 293.15K and pressure of 1bar (energy equation not solved). Although Diesel is utilized as test fuel in the current work, the results can be considered valid for low viscosity fuels as long as the Ohnesorge number is kept below 0.1 [59]. The same is true for the effect of ambient pressure or equivalently that of the density ratio, which becomes important approximately below 32 [53, 60]. Both the properties of Diesel and air as well as the droplet diameter are based on [61] as presented in Table 3. The

corresponding non-dimensional numbers are ε=678, *Oh*=0.038 and *N*=117 (eq. (3)). The high density ratio (ε) and low *Oh* number ensure that their effect is minimized, focusing only on the effect of *We* number. By altering the gas velocity, the resulting *We* numbers range from 20 up to 350, resulting in 21 simulations in the three breakup regimes, i.e. those of bag, multi-mode and sheet-thinning, as shown in Table 4. The corresponding *Re* numbers range from 531 to 2221.

Table 3. Properties of liquid Diesel and air at *T*=293.15K and *P*=1bar based on [61].

D_0 (μm)	*P* (bar)	T_g (K)	μ_g(kg/s·m)	ρ_g (kg/m^3)	T_L (K)	μ_L(kg/m·s)	ρ_L(kg/m^3)	σ (N/m)
198	1	293.15	1.85E-05	1.215	293.15	0.00217	824	0.02

Table 4. Examined cases of CFD simulations.

Case	$U_{g,0}$ (m/s)	*We*	*Re*	*Oh*	ε	*N*
1	40.8	20	531	0.038	678	117
2	43.7	23	569	0.038	678	117
3	49.1	29	639	0.038	678	117
4	53.2	34	692	0.038	678	117
5	57.7	40	751	0.038	678	117
6	64.5	50	839	0.038	678	117
7	67.6	55	880	0.038	678	117
8	70.6	60	920	0.038	678	117
9	76.3	70	993	0.038	678	117
10	81.5	80	1062	0.038	678	117
11	86.5	90	1126	0.038	678	117
12	91.2	100	1187	0.038	678	117
13	95.6	110	1245	0.038	678	117
14	99.9	120	1300	0.038	678	117
15	103.9	130	1354	0.038	678	117
16	107.9	140	1405	0.038	678	117
17	111.7	150	1454	0.038	678	117
18	128.9	200	1679	0.038	678	117
19	144.1	250	1877	0.038	678	117
20	157.9	300	2056	0.038	678	117
21	170.6	350	2221	0.038	678	117

3 Mathematical model

3.1 Non-dimensional numbers

The non-dimensional numbers that are commonly used to describe the breakup of isolated droplets are the Weber (*We*), Ohnesorge (*Oh*) and Reynolds (*Re*) numbers as well as the density (ε) and viscosity ratios (*N*) of the two phases [59].

$$We = \frac{\rho_g U_0^2 D_0}{\sigma} \qquad Oh = \frac{\mu_L}{\sqrt{\rho_L \sigma \mathrm{D}_0}} \qquad Re = \frac{\rho_g U_0 D_0}{\mu_g} \qquad \varepsilon = \frac{\rho_L}{\rho_g} \qquad N = \frac{\mu_L}{\mu_g} \quad (1)$$

The breakup timescale proposed by Nicholls and Ranger [62] is used as a convenient non-dimensionalisation parameter for time ($t^*=t/t_{sh}$):

$$t_{sh} = \frac{\mathrm{D}_0}{U_0}\sqrt{\varepsilon} \tag{2}$$

Finally, the non-dimensional droplet deformation (y), which is the quantity of most importance in this work, is quantitively described by the non-dimensional cross-stream diameter of the droplet (D_{cr}/D_0), as shown in Figure 2.

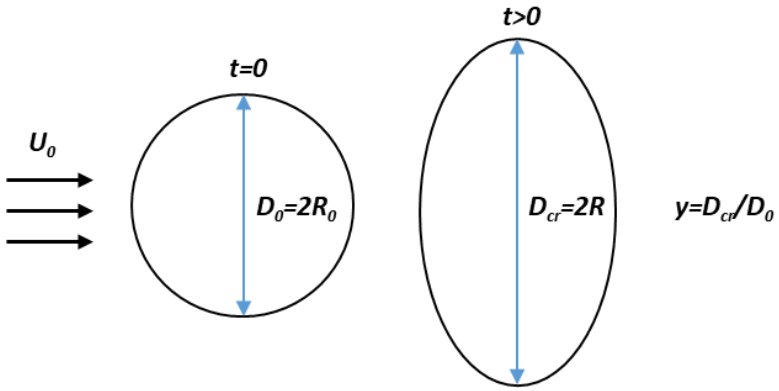

Figure 2. Definition of the cross-stream droplet diameter and the non-dimensional droplet deformation.

3.2 Improved TAB model

O'Rourke and Amsden [43] derived the differential equation of the TAB model for the displacement of the drop equator compared to that of a spherical shape. By introducing the non-dimensional droplet deformation (y) and time (t^*), as well as the *We* and *Oh* numbers the equation becomes:

$$\ddot{y} + 4C_d\frac{Oh}{\sqrt{We}}\dot{y} + \frac{8C_k}{We}(y-1) = 4C_F \tag{3}$$

where $\dot{y} = dy/dt^*$ is the dimensionless deformation rate and $\ddot{y} = d^2y/dt^{*2}$ the dimensionless deformation acceleration.

The parameters of the improved TAB model (C_k and C_f) are found by fitting to the results for the temporal evolution of droplet deformation of a) the experimental studies of [12, 18-21] (bag regime) and b) the results of the CFD simulations (multi-mode and sheet-thinning regimes), as presented in Table 5 along with those of the original TAB of [26]. The value of zero for the surface tension term C_k was found to fit better to the aforementioned group of results for $We \geq 60$, something that results in the negation of the surface tension term in the modified TAB model (eq. (3)). Thus, its solution for the droplet deformation results in an exponential function of time instead of an oscillation. The physical interpretation of this, is that for high *We* numbers the aerodynamic forces are much higher than the surface tension forces, and therefore the latter can be neglected. Finally, the value of the viscosity

parameter C_d is taken constant and equal to 10, in agreement with [29, 63]; this parameter is expected to be a function of *Oh* number, which has a constant low value throughout this study and has a minor effect on the breakup process.

Table 5. Parameters of the original and improved TAB models.

Breakup mode	Original TAB			Improved TAB		
	C_d	C_f	C_k	C_d	C_f	C_k
Bag	5	1/3	8	10	$0.13 + 0.0026We$	$-1.32 + 0.12We$
Multi-mode				10	$0.46 + 0.0022We$	$7.87 - 0.13We$, *We*<60
Sheet-thinning						0, *We*≥60

3.3 Modified Navier-Stokes (M-NS) model

In this work we introduce a numerical improvement of the bag-NS breakup model, which has been developed in [19]; however, its derivation is repeated in Appendix C due to an erroneous calculation, which is corrected in this work. This is the multiplier of the viscosity term (2nd term from the left of eq. (28)), which is found equal to 16 in this work, while in [19] it was estimated equal to 8, probably due to a miscalculation in the algebraic manipulations. Either way, the contribution of this term in the calculation of the droplet deformation is low for the current examined conditions of low *Oh* numbers (*Oh*<0.04) and thus it is not affecting the results. However, its contribution is expected to increase at higher *Oh* numbers.

In the M-NS model the droplet deformation is described by equation (4). The difference with the original bag-NS model lies in the estimation of the pressure term, which is a function of y^n instead of y (4th term from the left of eq. (4)). Eq. (4) is a second-order non-linear differential equation with no analytical solution, the numerical solution of which is obtained in this work using an explicit 4th order Runge-Kutta method [64, 65].

$$\ddot{y} + 16\frac{Oh}{\sqrt{We}}\frac{1}{y^2}\dot{y} + \frac{24}{We}y - \frac{a^2}{4}y^n = 0 \quad (4)$$

The parameter *a* is called rate of stretching, while the parameter *n* is called pressure exponent and has been introduced in the present work to provide a more flexible numerical consideration of the pressure contribution. For *n*≥1 the deformation grows exponentially in time (note that *n*=1 corresponds to the original model of [19], as shown in Table 6), while for n<1 the deformation becomes oscillatory. More specifically, for *n*=0 the equation becomes similar to that of the TAB model, while for *n*=-1 it becomes similar to that of the NLTAB, since the pressure term is proportional to *1/y*. For each breakup mode, the value of *n* that gives the higher coefficient of determination (R^2) is selected, compared to the results of the experimental studies of [12, 18-21] (bag regime) and the CFD simulations (multi-mode and sheet-thinning regimes), as shown in Table 6.

Finally, instead of using a constant value for the parameter *a,* the current study proposes this to be a function of the *We* number for each breakup mode (bag, multi-mode and sheet-thinning), as presented in Table 6. For the bag breakup regime, the experimental data of [12, 18-21] for the temporal evolution

of droplet deformation are utilized, while for the multi-mode and sheet-thinning regimes the results of the CFD simulation are employed instead; α is found for each *We* number by fitting eq. (4) to the results and by assuming a linear dependence on the *We* number. It should be mentioned that the equation of α in the bag breakup regime gives a value of a equal to 2.88 for *We*=15, which is close to the value of 2.83 proposed by [19] for the same *We* (Table 6).

Table 6. Parameters of the bag-NS and M-NS models.

Breakup mode	Original bag-NS		Proposed M-NS	
	n	α	n	α
Bag	1	2.83	1	$3.6 - 0.048We$
Multi-mode	-	-	-0.5	$3.35 + 0.0032We$
Sheet-thinning	-	-	2	$2.35 + 0.0042We$

3.4 Breakup condition

Most breakup models of the literature assume a constant critical deformation (onset of breakup) in the range of 1.8 to 2.1 (see Table 2), with the exception of the BTB model in which the critical deformation is a function of *We*. In this study we assume that the breakup occurs when either the maximum deformation is reached ($\dot{y}$=0) or when a critical deformation is exceeded (y_{cr}=3.5), whichever comes first. The condition of y_{cr}=3.5 is calculated based on the results of the CFD simulations for a range of *We* numbers from 20 up to 350 and it is also in agreement with the experimental data of [18] for a *We* number equal to 20, as shown in Figure 3. The critical deformation of the various models of the literature is presented in the figure as well.

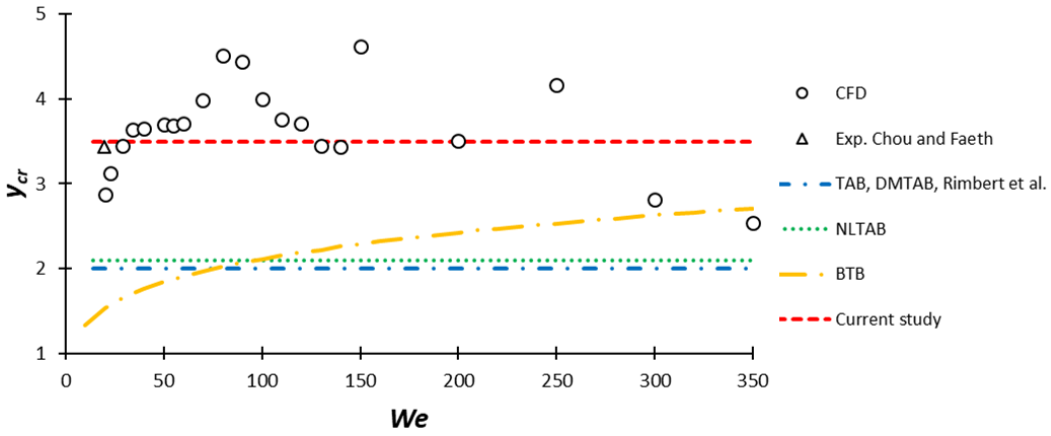

Figure 3. Critical deformation as estimated by the CFD simulations and the experiments of [18], as well as the assumptions of the various breakup models.

4 Results and discussion

The temporal evolution of droplet deformation can be calculated using the two models (improved TAB and M-NS) with their respective equations and parameters: i) improved TAB model using eq. (3) and the parameters of Table 5 and ii) M-NS model using eq. (4) and the parameters of Table 6. The results

are presented in the following sub-sections as calculated by the two models in the bag, multi-mode and sheet-thinning regimes, against the results of experimental studies (bag breakup regime) and those of the CFD simulations (multi-mode and sheet-thinning regimes).

4.1 Bag breakup regime - *We*=10-20

The results of two breakup models (improved TAB and M-NS) are illustrated in Figure 4 for two *We* numbers in the bag breakup regime (*We*=15 and 20), along with those of the experimental studies for the same *We* numbers [12, 18-21]. Both models show a good agreement with the experimental data for both *We* numbers. The TAB model predicts lower values for the deformation compared to the M-NS model at higher t^*(≥2.5), owing to the assumption that the droplet deformation is modeled as an oscillation in the TAB model, in comparison with the exponential behavior predicted by the M-NS model. It should be noted that the experimental data of Chou and Faeth [18] exhibit a fluctuation for the case of *We*=20 and at t^*≥2, something that pertains to a combined exponential and oscillatory droplet deformation. This behavior is also observed in the simulations of Figure 5 and Figure 6 and it is something that has not been reported before in the literature. Nevertheless, the exponential part seems to dominate, while further experimental and numerical studies are required to verify this observation.

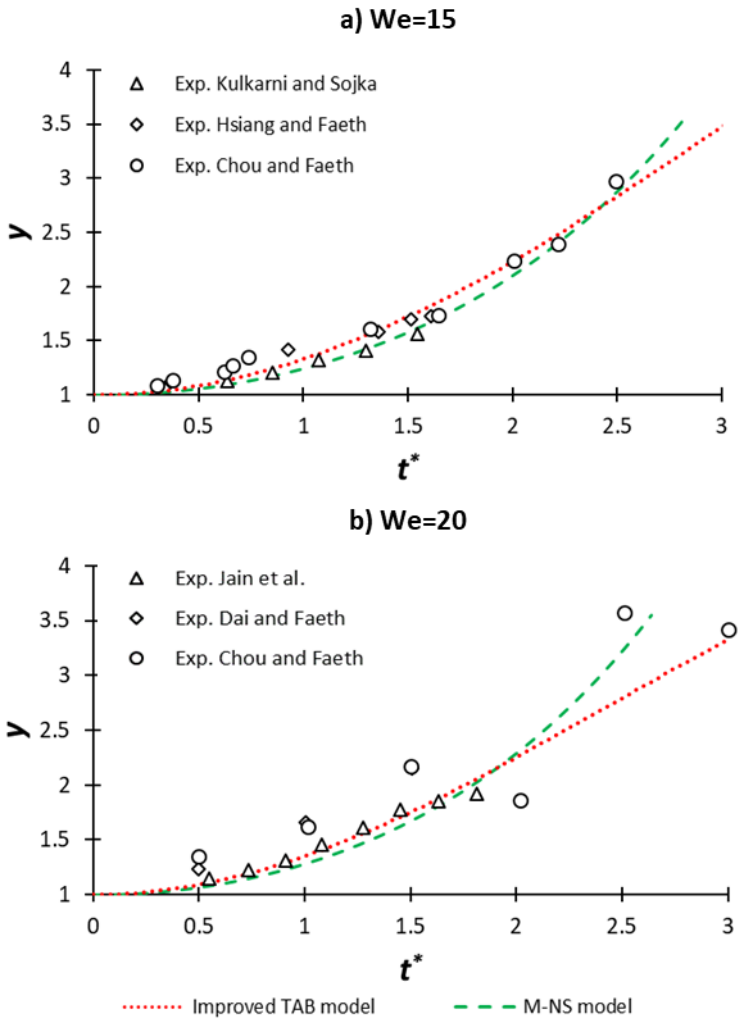

Figure 4. Temporal evolution of droplet deformation as predicted by the improved TAB and M-NS models along with the experimental data from the literature for a) *We*=15 and b) *We*=20.

4.2 Multi-mode breakup regime - *We*=21-65

The results of the two breakup models are presented in Figure 5 for two *We* numbers, 23 and 60, in the multi-mode regime, along with those of the simulations for the same *We* numbers. The agreement is good between the models and the simulations, apart from the prediction of a slightly higher breakup initiation time for the case of *We*=23. This is attributed to the oscillatory behavior of the models and the consequent occurrence of breakup at the time when $\dot{y}$=0 and not at y_{cr}=3.5. Note that a selection of an exponential solution for the M-NS model (parameter $n \geq 1$), although it gives slightly better results for the case of *We*=60, it does not agree will with the simulations for the case of *We*=23, and therefore is not selected.

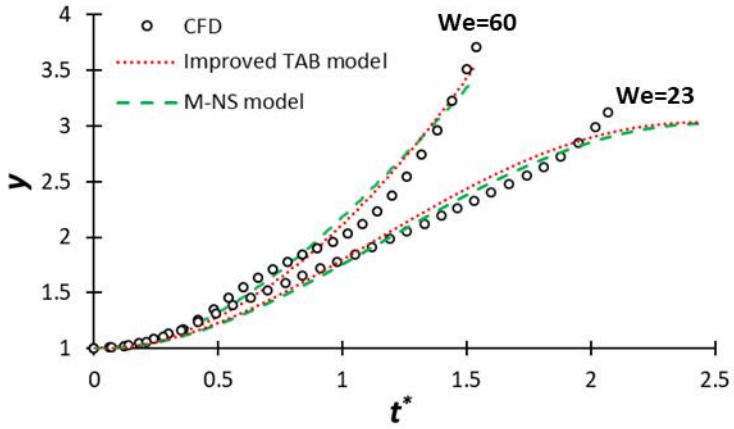

Figure 5. Temporal evolution of droplet deformation as predicted by the improved TAB and M-NS models with the results of the simulations for two *We* numbers in the multi-mode regime (60 and 23).

4.3 Sheet-thinning breakup regime - *We*=66-350

In Figure 6 the results from the two breakup models are presented for two *We* numbers (80 and 250) in the sheet-thinning regime, along with those of the simulations for the same *We* numbers. Good agreement is observed again for both models, although a slight underestimation of y_{cr} is noticed for both *We* numbers, due to the higher value of y_{cr} as predicted by the simulations in the current regime. In addition, the results of the M-NS model are closer to those of the simulations due to their steeper inclination.

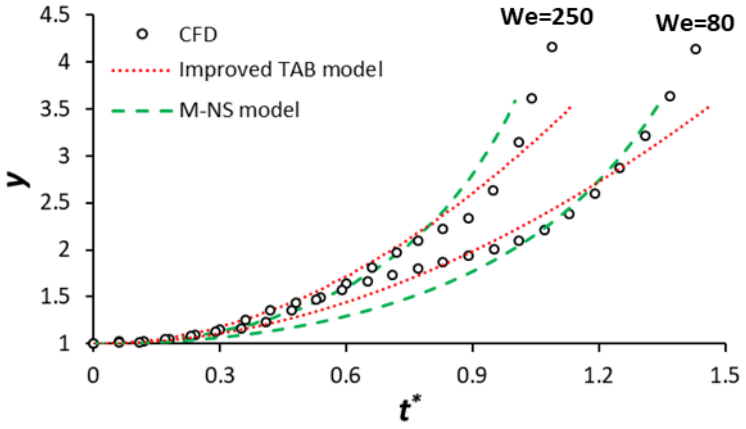

Figure 6. Temporal evolution of droplet deformation as predicted by the improved TAB and M-NS models along with the results of the simulations for two *We* numbers in the sheet-thinning regime (80 and 250).

5 Conclusions and future work

The present work examined the droplet deformation and breakup models for the three basic regimes of droplet breakup, i.e. the bag, multi-mode and sheet-thinning. The publicly available empirical models of [18, 20, 23, 24] were examined as well as the theoretical models TAB, DDB, NLTAB, Rimbert et al. [36] and bag-NS [19], for their range of validity against available experimental data (*We*=15-101). It was found (see Appendix A) that none of them was capable of accurately predicting the droplet

deformation in all the three breakup regimes. For this reason, two existing models were improved and modified, namely i) an improved TAB model and ii) the M-NS model, which is a modified version of an existing model based on the Navier-Stokes equations.

The parameters of both models were estimated for each breakup regime, based both on experimental data found in the literature (bag regime) and CFD simulations with Diesel droplets performed as part of this study in the multi-mode and sheet-thinning breakup regimes, for which available experimental data are not enough to cover the entire range of values for the necessary parameters. In addition, a breakup condition was introduced ($\dot{y}$=0 or y_{cr}=3.5) based on the results of the CFD simulations and those of the experiments, which gives acceptable results for all examined cases.

Regarding the prediction of droplet deformation, both models showed a good agreement against the experimental data in the bag breakup regime and the CFD simulations in the multi-mode and sheet-thinning regimes, with the M-NS model showing the best performance overall.

It should be noted that the proposed parameters and breakup conditions for both models are valid for low *Oh* (low viscosity fuels), high ε and for isolated droplets, and thus a separate investigation is required for the estimation of the parameters at different conditions. Finally, a unified secondary breakup model is introduced, which consolidates into a single equations various models of the literature (TAB, NLTAB, DDB and NS), by using adjustable coefficients (see Appendix B). As a future work, the parameters of this model can be estimated based on CFD simulations, which in return may result in the formulation of a completely new deformation and breakup model.

Acknowledgements

Financial support from the MSCA-ITN-ETN of the European Union's H2020 programme, under REA grant agreement n. 675676 is acknowledged.

Appendix A. Comparison of the existing deformation and breakup models with experimental data.

The temporal evolution of droplet deformation as predicted by the various models of Table 1 and selected models of Table 2 are presented in Figure 7 and Figure 8, respectively, along with various experimental data found in the literature in three breakup regimes (bag, multi-mode and sheet-thinning) for *We*=15 [18-20], *We*=20 [12, 18, 21], *We*=52.6 [22] and *We*=101 [22]. It should be noted that the applicability of some models has been extended beyond the range presented in Table 1 and Table 2 in order to assess if their range of applicability can be extended. The experiments are plotted up to the breakup initiation time, while those by [22] have been shifted in terms of time based on the results of CFD simulations at the same conditions. In the bag breakup regime (*We*=15-20) the empirical model of Chou and Faeth [18] and the theoretical model of Kulkarni and Sojka [19] show the best agreement, in the multi-mode regime (*We*=52.6) that of Cao et al. [23] and the DDB, and in the sheet-thinning regime (*We*=101) that of Gel'fand et al. [24] and the DDB again.

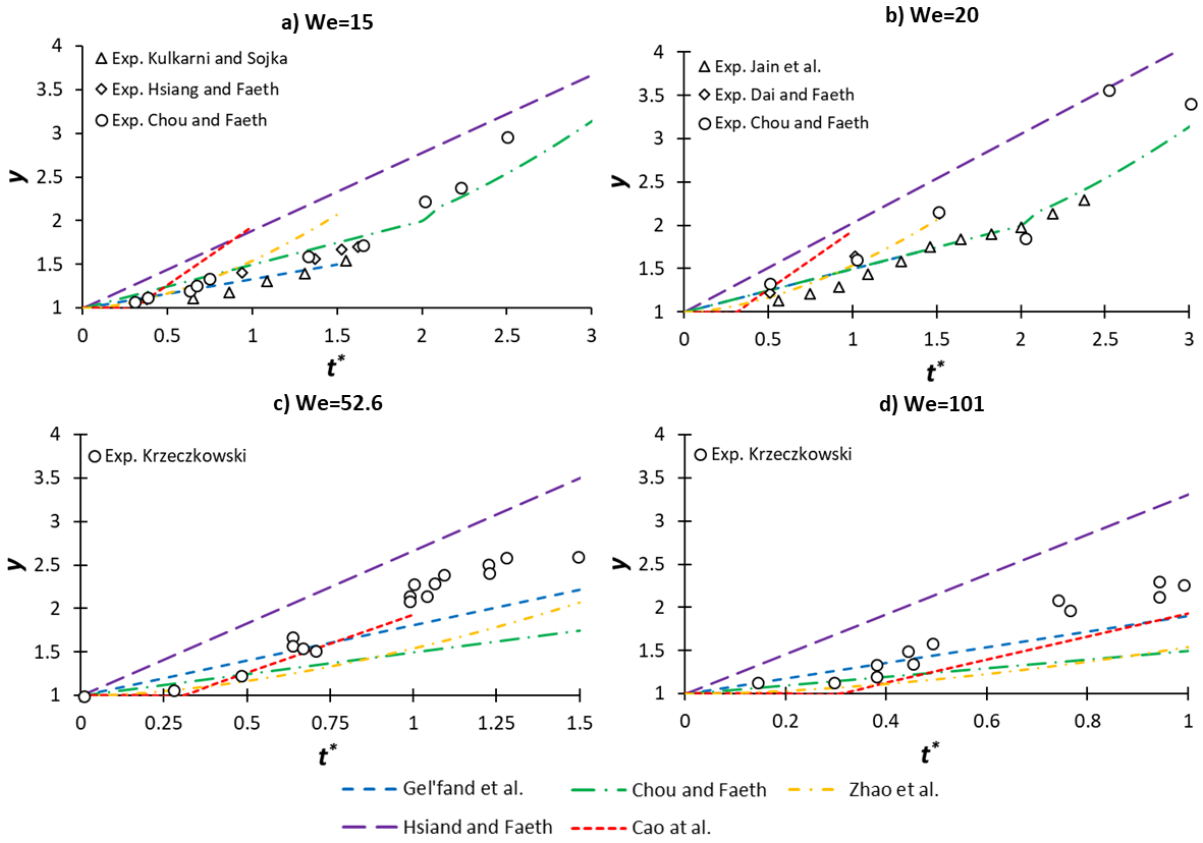

Figure 7. Comparison between experimental data and the predictions of the various empirical models for the temporal evolution of droplet deformation for a) *We*=15, b) *We*=20, c) *We*=52.6 and d) *We*=101.

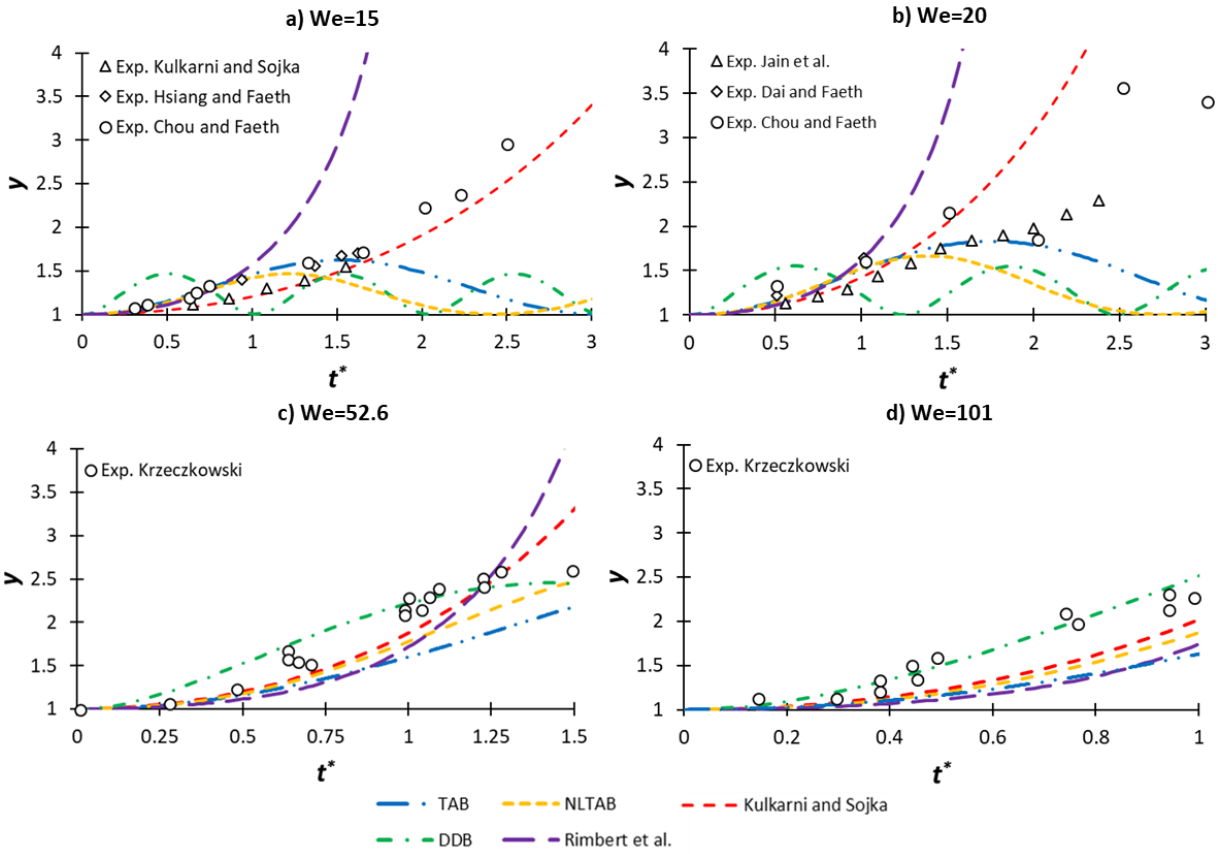

Figure 8. Comparison between experimental data and the predictions of the various theoretical models for the temporal evolution of droplet deformation for a) *We*=15, b) *We*=20, c) *We*=52.6 and d) *We*=101.

Appendix B. Unified secondary breakup model.

In order to develop the unified secondary breakup model, a similar procedure to that of Schmehl at al. [37] for the derivation of the NLTAB model is followed, but the appearing terms are expressed in a more generic way. This is accomplished by utilizing basic equations, (e.g. the work is given by the multiplication of a force with an area), along with reference values for these variables (e.g. reference force and area). In addition, adjustable parameters are introduced to account for the effects of physical parameters/mechanisms that are not included in the equations, since they are expressed by using reference magnitudes, such as the internal flow in the droplet and the pressure distribution around it. For convenience the mechanical energy balance of the droplet is employed first, which is written in rate form in eq. (5):

$$\frac{dE_d}{dt} = \dot{W}_{press} - \dot{W}_{vis,d} \tag{5}$$

The droplet energy consists of three parts, i.e. a) the kinetic translational energy, b) the surface energy and c) the kinetic energy as the droplet deforms. It should be noted also that heat transfer effects could be also added in eq. (5), which are not within the scope of the current work and therefore are neglected. It is mathematically proved that the translational droplet energy cancels the work of

pressure forces in the direction of the flow, using the droplet momentum equation in the streamwise direction. Thus, the translational terms will not be included.

Starting with the kinetic energy this can be calculated as:

$$E_{kin,d} = f_{kin}\frac{1}{2}m_L U_{def,y}^2 = f_{kin}\frac{1}{2}\rho_L\frac{\pi D_0^3}{6}\left(\frac{dR}{dt}\right)^2 \quad (6)$$

The term $U_{def,y}=dR/dt$ denotes the deformation velocity in the cross-stream direction and serves as a scaling velocity for the calculation of the kinetic energy, while the coefficient f_{kin} is used to include the secondary effects appearing during droplet deformation. These are: i) the secondary kinetic energy arising from the axial (transverse) deformation, ii) the variation of liquid velocity along the cross-stream diameter (it is 0 at the symmetry axis and *dR/dt* at the peripheral tip), and iii) the internal liquid flow/circulation. In the TAB and DDB models the value of f_{kin} is equal to 1, while in the NLTAB it is a decreasing function of *y* (see Table 7).

The rate of kinetic energy is:

$$\frac{dE_{kin,d}}{dt} = \frac{1}{2}\rho_L\frac{\pi D_0^3}{6}\left(f_{kin}2\frac{dR}{dt}\frac{d^2R}{dt^2} + \frac{df_{kin}}{dR}\left(\frac{dR}{dt}\right)^3\right) \quad (7)$$

And by introducing the non-dimensional numbers: $y = \frac{2R}{D_0} \rightarrow R = y\frac{D_0}{2}$ (see Figure 2) and $t^* = \frac{t}{D_0\sqrt{\varepsilon}}U_0 \rightarrow t = t^*\frac{D_0\sqrt{\varepsilon}}{U_0}$, the equation becomes ($\dot{y} = \frac{dy}{dt^*}$):

$$\frac{dE_{kin,d}}{dt} = \frac{2}{3}\left(\frac{\rho_g\pi D_0^2 U_0^3}{16\sqrt{\varepsilon}}\right)\left(f_{kin}\dot{y}\ddot{y} + \frac{1}{2}\frac{df_{kin}}{dy}(\dot{y})^3\right) \quad (8)$$

Next, the rate of surface energy is given in eq. (9):

$$\frac{dE_{surf,d}}{dt} = \frac{d}{dt}(\sigma S) = \sigma\frac{dS}{dy}\frac{dy}{dt} = \sigma\pi D_0^2\frac{dS^*}{dy}\frac{dy}{dt} \quad (9)$$

where S^* represents the dimensionless droplet surface ($S^* = S/\pi D_0^2$).

Introducing the non-dimensional time (t^*) the equation becomes:

$$\frac{dE_{surf,d}}{dt} = \sigma\pi D_0^2\frac{dS^*}{dy}\frac{dy}{dt^*\frac{D_0\sqrt{\varepsilon}}{U_0}} = \frac{\sigma\pi D_0 U_0}{\sqrt{\varepsilon}}\frac{dS^*}{dy}\dot{y} = \left(\frac{\rho_g\pi D_0^2 U_0^3}{16\sqrt{\varepsilon}}\right)\frac{16}{We}\frac{dS^*}{dy}\dot{y} \quad (10)$$

In eq. (9), the term dS^*/dy is a characteristic of the droplet shape and depends on the breakup mode and breakup phase (e.g. flattening phase, bag creation, etc). The majority of the breakup models assumed ellipsoid shape (either cylinder or axisymmetric, see Table 2) and provided the term dS^*/dy as a function of the instantaneous deformation y, using either a simplified analytic formula or a

polynomial fitting. Although the assumption of an ellipsoidal shape is an oversimplification it reflects with low error the droplet surface area when compared with the results of CFD (comparison not presented here).

For the pressure work term, it is assumed that this is obtained by multiplying a reference force (F_{ref}) with the reference deformation velocity $U_{def,y}$:

$$\dot{W}_{press} = f_{press} \cdot F_{ref} \cdot U_{def,y} = f_{press} \frac{1}{2} \rho_g u_{rel}^2 \frac{\pi D_0^2}{4} \frac{dR}{dt} \tag{11}$$

The introduction of non-dimensional numbers: y, t^* and $u_{rel}^* = \frac{u_{rel}}{U_0}$, gives:

$$\dot{W}_{press} = f_{press} \left(\frac{\rho_g U_0^3 \pi D_0^2}{16\sqrt{\varepsilon}} \right) u_{rel}^{*2} \dot{y} \tag{12}$$

The coefficient f_{press} is used to account for the effect of pressure distribution around the droplet as also the change of frontal area during droplet deformation. In the NLTAB model this term is proportional to $\dot{y}/y$, while in the model of Rimbert et al. is proportional to $K_P(y) \cdot \dot{y}$, where K_P is a polynomial function of y (see Table 7). The term u_{rel}^* includes the effect of change of the relative drop-gas velocity; the inclusion of this effect implies that an additional equation has to be solved for the droplet motion (see [16]), while ignoring this effect, implies that u_{rel}^* is unity. The CFD simulations showed that $u_{rel}^* \geq 0.8$ for all examined cases even at the instance of breakup, where it takes its minimum value.

Finally, for the viscous dissipation term the approximation of NLTAB [37] is used (n is the unit vector in the direction of y):

$$\dot{W}_{vis,d} = f_{vis} 12 \mu_L \left(\frac{\partial u_{cm}}{\partial n} \right)^2 \frac{\pi D_0^3}{6} = f_{vis} 2 \mu_L \left(\frac{1}{y} \frac{dy}{dt} \right)^2 \pi D_0^3 \tag{13}$$

With the introduction of the non-dimensional time (t^*) and the numbers *We* and *Oh*, the equation becomes:

$$\dot{W}_{vis,d} = f_{vis} \left(\frac{\rho_g \pi D_0^2 U_0^3}{16\sqrt{\varepsilon}} \right) 32 \frac{Oh}{\sqrt{We}} \left(\frac{\dot{y}}{y} \right)^2 \tag{14}$$

The coefficient f_{vis} is used to account for the effect of energy dissipation in the streamwise direction.

By substituting equations (8), (10), (12) and (14) into (5), the final expression for y is derived in (15). One more coefficient has been added to the equation for the effect of surface energy (f_{st}) and all constants have been incorporated inside the parameters.

$$\left(f_{kin} \ddot{y} + \frac{1}{2} \frac{df_{kin}}{dy} \dot{y}^2 \right) + f_{vis} \frac{Oh}{\sqrt{We}} \frac{\dot{y}}{y^2} + \frac{f_{st}}{We} \frac{dS^*}{dy} = f_{press} u_{rel}^{*2} \tag{15}$$

By giving the appropriate values to the parameters f_{kin}, f_{vis}, f_{st}, f_{press}, dS^*/dy and u^*_{rel}, equation (15) matches the equations of the models TAB, NLTAB, DDB and NS, as shown in Table 7. Finally, the values of the coefficients can be estimated based on the results of the CFD simulations resulting in a completely new model. However, their derivation is complex and is still a work in progress.

Table 7. Parameters of the unified secondary breakup model to match the various models of the literature.

	TAB	**NLTAB**	**DDB**	**Bag-NS**	**M-NS**
f_{kin}	1	$\frac{\pi^2+\frac{16}{y^6}}{\pi^2+16}$	1	1	1
f_{vis}	$4y^2C_d$, C_d=5	40	$9\pi^2$	16	16
f_{st}	$8C_k$, C_k=8	29	$\frac{27\pi^2}{2}$	24	24
f_{press}	$4C_F$, C_f=1/3	$\frac{2C_2}{y}$, C_2=2/3	$9\pi/8$	$\frac{a^2}{4}y$, $a=2\sqrt{2}$	$\frac{a^2}{4}y^n$, $a=f(We)$
$\frac{dS^*}{dy}$	$y-1$	Ellipsoid	$(1-2y^{-6})y$	y	y
u^*_{rel}	1	1	1	1	1

Appendix C. Derivation of the bag-NS model.

Initially, the viscous Navier-Stokes equations in cylindrical axisymmetric coordinates are employed (see Figure 9):

$$\rho_L\left(\frac{\partial u_r}{\partial t}+u_r\frac{\partial u_r}{\partial r}\right)=-\frac{\partial p}{\partial r}+\mu_L\left[\frac{1}{r}\frac{\partial}{\partial r}\left(r\frac{\partial u_r}{\partial r}\right)-\frac{u_r}{r^2}\right] \tag{16}$$

$$r\frac{\partial h}{\partial t}+\frac{\partial(ru_rh)}{\partial r}=0 \tag{17}$$

Moreover, the mass conservation gives the rim thickness as:

$$h(t)=\frac{D_0^3}{6R^2} \tag{18}$$

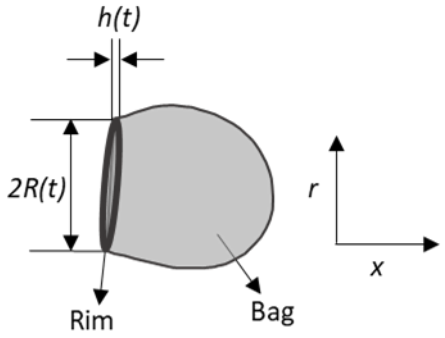

Figure 9. Definition of rim thickness and droplet radius in cylindrical coordinates.

The parameter u_r is found by substituting eq. (18) into (17) and solving for it:

$$u_r = \frac{r}{R}\frac{dR}{dt} \tag{19}$$

Eq. (16) requires the calculation of the pressure gradient (*dp/dr*). First, the normal stress balance across the interface is employed:

$$\sigma\kappa = T_{rr}(g) - T_{rr}(l) \tag{20}$$

T_{rr} *(l)* and T_{rr} *(g)* represent the normal stress components associated with the liquid and the surrounding gas, given by $-p_L(r) + 2\mu_L\frac{\partial u_r}{\partial r}$ and $-p_g(r)$, respectively. At *r=R* equation (20) gives:

$$p_L(R) = p_g(R) + \sigma\kappa + 2\mu_L\frac{\partial u_r}{\partial r} \tag{21}$$

The gas pressure field around the droplet (p_g) can be estimated using the momentum and mass conservation in the gas phase, with the assumptions of inviscid flow, incompressible fluid and quasi-steady state. Moreover, the local gas flow is assumed to have the structure of a stagnation point: $U_x = -aU_x/D_0$, where *a* is an indicator of the rate of stretching. The resulting equation is (22):

$$p_g(r,x) = p_g(0) - \rho_g\frac{a^2U_0^2}{8D_0^2}r^2 + \rho_g\frac{a^2U_0^2}{8D_0^2}x^2 \tag{22}$$

At *x=0* eq. (22) becomes:

$$p_g(r) = p_g(0) - \rho_g\frac{a^2U_0^2}{8D_0^2}r^2 \tag{23}$$

$p_g(0)$ is the stagnation pressure at $r = x = 0$ given by $p_g(0)=\rho_g U_0^2/2$. Substituting eq. (23) and (19) into (21) gives:

$$p_L(R) = p_g(0) - \rho_g \frac{a^2 U_0^2}{8 D_0^2} R^2 + \frac{2\sigma}{h} + 2\mu_L \frac{\partial u_r}{\partial r} \tag{24}$$

The curvature is given by $k = \left(\frac{h(t)}{2}\right)^{-1}$ due to the rounded periphery of the liquid disk. The pressure gradient can finally be calculated using eqs. (24) and (18) as:

$$\frac{\partial p}{\partial r} \approx \frac{p_L(R) - p_g(R)}{R} = \frac{1}{R}\left(-\rho_g \frac{a^2 U_0^2}{8 D_0^2} R^2 + \frac{12\sigma}{D_0^3} R^2 + \frac{2\mu_L}{R}\frac{dR}{dt}\right) \tag{25}$$

Substituting eqs. (25) and (19) into (16):

$$\rho_L \frac{r}{R}\frac{d^2 R}{dt^2} = -\frac{1}{R}\left(-\rho_g \frac{a^2 U_0^2}{8 D_0^2} R^2 + \frac{12\sigma}{D_0^3} R^2 + \frac{2\mu_L}{R}\frac{dR}{dt}\right) \tag{26}$$

The integration from $r=0$ to $r=R$ gives:

$$\frac{d^2 R}{dt^2} = \left(\rho_g \frac{a^2 U_0^2}{\rho_L 4 D_0^2} - \frac{24\sigma}{\rho_L D_0^3} - \frac{4\mu_L}{\rho_L R^3}\frac{dR}{dt}\right) R \tag{27}$$

Finally, the non-dimensional parameters are introduced: *We*, *Oh*, $y = R/(\frac{D_0}{2})$, $t^* = t/t_{sh} \Rightarrow t = t^* \frac{D_0\sqrt{\varepsilon}}{U_0}$, and the final differential equation for the droplet deformation is given in (28):

$$\ddot{y} + 16\frac{Oh}{\sqrt{We}}\frac{\dot{y}}{y^2} + \frac{24}{We} y = \frac{a^2}{4} y \tag{28}$$

References

[1] Ashgriz, N., 2011, Handbook of atomization and sprays: theory and applications, Springer Science & Business Media.

[2] "ANSYS®FLUENT Theory Guide, 2014, Release 16.0."

[3] Temkin, S., and Ecker, G. Z., 1989, "Droplet pair interactions in a shock-wave flow field," Journal of Fluid Mechanics, 202, pp. 467-497.

[4] Pilch, M., and Erdman, C. A., 1987, "Use of breakup time data and velocity history data to predict the maximum size of stable fragments for acceleration-induced breakup of a liquid drop," International Journal of Multiphase Flow, 13(6), pp. 741-757.

[5] Hsiang, L. P., and Faeth, G. M., 1995, "Drop deformation and breakup due to shock wave and steady disturbances," International Journal of Multiphase Flow, 21(4), pp. 545-560.

[6] Warnica, W. D., Renksizbulut, M., and Strong, A. B., 1995, "Drag coefficients of spherical liquid droplets Part 1: Quiescent gaseous fields," Experiments in Fluids, 18(4), pp. 258-264.

[7] Feng, Z.-G., and Michaelides, E. E., 2001, "Drag coefficients of viscous spheres at intermediate and high Reynolds numbers," Journal of Fluids Engineering, 123(4), pp. 841-849.

[8] Quan, S., and Schmidt, D. P., 2006, "Direct numerical study of a liquid droplet impulsively accelerated by gaseous flow," Physics of Fluids (1994-present), 18(10), p. 102103.

[9] Wadhwa, A. R., Magi, V., and Abraham, J., 2007, "Transient deformation and drag of decelerating drops in axisymmetric flows," Physics of Fluids (1994-present), 19(11), p. 113301.
[10] Khare P., V. Y., "Drag Coefficients of Deforming and Fragmenting Liquid Droplets," Proc. ILASS Americas, 25th Annual Conference on Liquid Atomization and Spray Systems.
[11] Kékesi, T., Amberg, G., and Prahl Wittberg, L., 2014, "Drop deformation and breakup," International Journal of Multiphase Flow, 66, pp. 1-10.
[12] Jain, M., Prakash, R. S., Tomar, G., and Ravikrishna, R. V., 2015, "Secondary breakup of a drop at moderate Weber numbers," Proceedings of the Royal Society A: Mathematical, Physical and Engineering Science, 471(2177).
[13] Strotos, G., Malgarinos, I., Nikolopoulos, N., and Gavaises, M., 2016, "Numerical investigation of aerodynamic droplet breakup in a high temperature gas environment," Fuel, 181, pp. 450-462.
[14] Yang, W., Jia, M., Sun, K., and Wang, T., 2016, "Influence of density ratio on the secondary atomization of liquid droplets under highly unstable conditions," Fuel, 174, pp. 25-35.
[15] Shao, C., Luo, K., and Fan, J., 2017, "Detailed numerical simulation of unsteady drag coefficient of deformable droplet," Chemical Engineering Journal, 308, pp. 619-631.
[16] Stefanitsis, D., Malgarinos, I., Strotos, G., Nikolopoulos, N., Kakaras, E., and Gavaises, M., 2017, "Numerical investigation of the aerodynamic breakup of Diesel and heavy fuel oil droplets," International Journal of Heat and Fluid Flow, 68, pp. 203-215.
[17] Stefanitsis, D., Malgarinos, I., Strotos, G., Nikolopoulos, N., Kakaras, E., and Gavaises, M., 2018, "Numerical investigation of the aerodynamic breakup of droplets in tandem," International Journal of Multiphase Flow.
[18] Chou, W. H., and Faeth, G. M., 1998, "Temporal properties of secondary drop breakup in the bag breakup regime," International Journal of Multiphase Flow, 24(6), pp. 889-912.
[19] Kulkarni, V., and Sojka, P., 2014, "Bag breakup of low viscosity drops in the presence of a continuous air jet," Physics of Fluids, 26(7), p. 072103.
[20] Hsiang, L. P., and Faeth, G. M., 1992, "Near-limit drop deformation and secondary breakup," International Journal of Multiphase Flow, 18(5), pp. 635-652.
[21] Dai, Z., and Faeth, G. M., 2001, "Temporal properties of secondary drop breakup in the multimode breakup regime," International Journal of Multiphase Flow, 27(2), pp. 217-236.
[22] Krzeczkowski, S. A., 1980, "Measurement of liquid droplet disintegration mechanisms," International Journal of Multiphase Flow, 6(3), pp. 227-239.
[23] Cao, X.-K., Sun, Z.-G., Li, W.-F., Liu, H.-F., and Yu, Z.-H., 2007, "A new breakup regime of liquid drops identified in a continuous and uniform air jet flow," Physics of Fluids, 19(5), p. 057103.
[24] Gel'Fand, B., Gubin, S., and Kogarko, S., 1974, "Various forms of drop fractionation in shock waves and their special characteristics," Journal of Engineering Physics and Thermophysics, 27(1), pp. 877-882.
[25] Zhao, H., Liu, H.-F., Xu, J.-L., Li, W.-F., and Lin, K.-F., 2013, "Temporal properties of secondary drop breakup in the bag-stamen breakup regime," Physics of Fluids, 25(5), p. 054102.
[26] O'Rourke, P. J., Amsden, A. A., and Society of Automotive, E., 1987, The tab method for numerical calculation of spray droplet breakup, Society of Automotive Engineers, Warrendale, PA.
[27] Lee, M. W., Park, J. J., Farid, M. M., and Yoon, S. S., 2012, "Comparison and correction of the drop breakup models for stochastic dilute spray flow," Applied Mathematical Modelling, 36(9), pp. 4512-4520.
[28] Kim, S., Hwang, J. W., and Lee, C. S., 2010, "Experiments and modeling on droplet motion and atomization of diesel and bio-diesel fuels in a cross-flowed air stream," International Journal of Heat and Fluid Flow, 31(4), pp. 667-679.
[29] Marek, M., 2013, "The double-mass model of drop deformation and secondary breakup," Applied Mathematical Modelling, 37(16-17), pp. 7919-7939.
[30] Villermaux, E., and Bossa, B., 2009, "Single-drop fragmentation determines size distribution of raindrops," Nature Physics, 5, p. 697.
[31] Opfer L. , I. V. R., C. Tropea, 2012, "Aerodynamic Fragmentation of Drops: Dynamics of the Liquid Bag," ICLASS 2012, 12th Triennial International Conference on Liquid Atomization and Spray SystemsHeidelberg, Germany.
[32] Detkovskii, D., and Frolov, S., 1994, "Model of the deformation of a liquid droplet in a gas flow," Journal of applied mechanics and technical physics, 35(6), pp. 911-919.
[33] Wang, C., Chang, S., Wu, H., and Xu, J., 2014, "Modeling of drop breakup in the bag breakup regime," Applied Physics Letters, 104(15), p. 154107.
[34] Wang, C., Chang, S., Wu, H., Ding, L., and Thompson, J., 2015, "Theoretical Modeling of Spray Drop Deformation and Breakup in the Multimode Breakup Regime," Atomization and Sprays, 25(10).
[35] Ibrahim, E., Yang, H., and Przekwas, A., 1993, "Modeling of spray droplets deformation and breakup," Journal of Propulsion and Power, 9(4), pp. 651-654.
[36] Rimbert, N., Hajjar, A., Castrillon-Escobar, S., Meignen, R., and Gradeck, M., 2014, "A New Look at the Droplet Deformation and Breakup Model," ILASS.
[37] Schmehl, R., 2002, "Advanced modeling of droplet deformation and breakup for CFD analysis of mixture preparation," Zaragoza, 9(11).
[38] Bartz, F., Schmehl, R., Koch, R., and Bauer, H., "An extension of dynamic droplet deformation models to secondary atomization," Proc. 23rd Annual Conference on Liquid Atomization and Spray Systems, Brno.

[39] Bartz, F., Guildenbecher, D., Schmehl, R., Koch, R., Bauer, H., and Sojka, P., "Model comparison for single droplet fragmentation under varying accelerations," Proc. 24th European conference on liquid atomization and spray systems.
[40] Sichani, A. B., and Emami, M. D., 2015, "A droplet deformation and breakup model based on virtual work principle," Physics of Fluids, 27(3), p. 032103.
[41] Wierzba, A., and Takayama, K., 1988, "Experimental investigation of the aerodynamic breakup of liquid drops," AIAA Journal, 26(11), pp. 1329-1335.
[42] Majithia, A., Hall, S., Harper, L., and Bowen, P., "Droplet breakup quantification and processes in constant and pulsed air flows," Proc. Proceedings of the 22nd Conference on Liquid Atomization and Spray Systems (ILASS-Europe), Como Lake, Italy.
[43] O'Rourke, P. J., and Amsden, A. A., 1987, "The TAB method for numerical calculation of spray droplet breakup," No. 0148-7191, SAE Technical Paper.
[44] Hirt, C. W., and Nichols, B. D., 1981, "Volume of fluid (VOF) method for the dynamics of free boundaries," Journal of Computational Physics, 39(1), pp. 201-225.
[45] Lafaurie, B., Nardone, C., Scardovelli, R., Zaleski, S., and Zanetti, G., 1994, "Modelling Merging and Fragmentation in Multiphase Flows with SURFER," Journal of Computational Physics, 113(1), pp. 134-147.
[46] "ANSYS®FLUENT, 2014, Release 16.0."
[47] Jain, S. S., Tyagi, N., Prakash, R. S., Ravikrishna, R., and Tomar, G., 2018, "Secondary breakup of drops at moderate Weber numbers: Effect of Density ratio and Reynolds number," arXiv preprint arXiv:1803.02989.
[48] Liang, C., 2016, "Computational methods for the investigation of liquid drop phenomena in external gas flows," PhD Open Access Dissertation, Michigan Technological University.
[49] Malgarinos, I., Nikolopoulos, N., and Gavaises, M., 2015, "Coupling a local adaptive grid refinement technique with an interface sharpening scheme for the simulation of two-phase flow and free-surface flows using VOF methodology," Journal of Computational Physics, 300, pp. 732-753.
[50] G. Strotos, I. M., N. Nikolopoulos, K. Papadopoulos, A. Theodorakakos, M.Gavaises, 2015, "Performance of VOF methodology in predicting the deformation and breakup of impulsively accelerated droplets," ICLASS 2015, 13th Triennial International Conference on Liquid Atomization and Spray Systems, August 23-27Tainan, Taiwan.
[51] Strotos, G., Malgarinos, I., Nikolopoulos, N., and Gavaises, M., 2016, "Predicting droplet deformation and breakup for moderate Weber numbers," International Journal of Multiphase Flow, 85, pp. 96-109.
[52] Strotos, G., Malgarinos, I., Nikolopoulos, N., and Gavaises, M., 2016, "Aerodynamic breakup of an n-decane droplet in a high temperature gas environment," Fuel, 185, pp. 370-380.
[53] Stefanitsis, D., Malgarinos, I., Strotos, G., Nikolopoulos, N., Kakaras, E., and Gavaises, M., 2017, "Numerical investigation of the aerodynamic breakup of Diesel droplets under various gas pressures," 28th Conference on Liquid Atomization and Spray Systems (ILASS-Europe 2017)Valencia, Spain.
[54] Malgarinos, I., Nikolopoulos, N., Marengo, M., Antonini, C., and Gavaises, M., 2014, "VOF simulations of the contact angle dynamics during the drop spreading: Standard models and a new wetting force model," Advances in Colloid and Interface Science, 212, pp. 1-20.
[55] Malgarinos, I., Nikolopoulos, N., and Gavaises, M., 2016, "A numerical study on droplet-particle collision dynamics," International Journal of Heat and Fluid Flow, 61, Part B, pp. 499-509.
[56] Malgarinos, I., Nikolopoulos, N., and Gavaises, M., 2017, "Numerical investigation of heavy fuel droplet-particle collisions in the injection zone of a Fluid Catalytic Cracking reactor, Part I: Numerical model and 2D simulations," Fuel Processing Technology, 156, pp. 317-330.
[57] Malgarinos, I., Nikolopoulos, N., and Gavaises, M., 2017, "Numerical investigation of heavy fuel droplet-particle collisions in the injection zone of a Fluid Catalytic Cracking reactor, part II: 3D simulations," Fuel Processing Technology, 156, pp. 43-53.
[58] Strotos, G., Malgarinos, I., Nikolopoulos, N., and Gavaises, M., 2016, "Predicting the evaporation rate of stationary droplets with the VOF methodology for a wide range of ambient temperature conditions," International Journal of Thermal Sciences, 109, pp. 253-262.
[59] Guildenbecher, D. R., López-Rivera, C., and Sojka, P. E., 2009, "Secondary atomization," Experiments in Fluids, 46(3), pp. 371-402.
[60] Aalburg, C., 2002, Deformation and breakup of round drops and nonturbulent liquid jets in uniform crossflows.
[61] Liu, Z., and Reitz, R. D., 1997, "An analysis of the distortion and breakup mechanisms of high speed liquid drops," International Journal of Multiphase Flow, 23(4), pp. 631-650.
[62] Nicholls, J. A., and Ranger, A. A., 1969, "Aerodynamic shattering of liquid drops," AIAA Journal, 7(2), pp. 285-290.
[63] Schlottke, M., 2011, "Analytical Investigation of Droplet Breakup in Accelerated Flow," PhD thesis, Universität Stuttgart.
[64] Dormand, J. R., and Prince, P. J., 1980, "A family of embedded Runge-Kutta formulae," Journal of computational and applied mathematics, 6(1), pp. 19-26.
[65] Shampine, L. F., and Reichelt, M. W., 1997, "The matlab ode suite," SIAM journal on scientific computing, 18(1), pp. 1-22.